Central European Science Journals
www.cesj.com

Central European Journal of Physics
Central European Science Journals
CEJP 2(4) 2004 645–659

Multiscale semicontinuous thin film descriptors

Jiří Boldyš[1,2] *, Rudolf Hrach[1] †

[1] *Department of Electronics and Vacuum Physics, Faculty of Mathematics and Physics, Charles University, V Holešovičkách 2, 180 00 Prague 8, Czech Republic*

[2] *Institute of Information Theory and Automation, Academy of Sciences of the Czech Republic, Pod vodárenskou věží 4, 182 08 Prague 8, Czech Republic*

Received 11 June 2004; revised 20 August 2004

Abstract: In experimental thin film physics, there is a demand to characterize a growing thin film or the thin film resulting from an experiment. While methods for discontinuous, island-like thin films have been developed, there is a lack of results directly applicable to semicontinuous thin film description. In this contribution, a unique combination of image processing methods is collected and further developed, which results in a novel set of semicontinuous thin film descriptors. In particular, the shape of the thin film contours and the thin film image intensity profiles are analyzed in a multiscale manner. The descriptiveness of the proposed features is demonstrated on a few thin film photographs from real experiments. This work establishes a basis for further measurement, description, simulation or other processing in the physics of semicontinuous thin films, using any direct imaging modality.
© Central European Science Journals. All rights reserved.

Keywords: semicontinuous thin films, wavelet transform, segmentation, skeleton, graph representation
PACS (2000): 68.55.Jk,02.30.Qy

1 Introduction

One of the most important tasks in thin film physics is thin film description. Both description of the final thin film product and monitoring of a growing thin film are important. There are many thin film imaging modalities available nowadays, e.g. TEM

* E-mail: boldys@utia.cas.cz
† E-mail: rudolf.hrach@mff.cuni.cz

or SEM. Typical thin film examples are shown in the section with experimental results.

Usually, in the initial stages, thin film images contain objects resembling drops. During further deposition, they undergo coalescence, in which they get larger and connected. Differences in thin film morphology (surface structure, spatial distribution, etc.) are due to different materials used and different physical conditions during an experiment.

Discontinuous thin film image description is a well elaborated field—see e.g. works devoted to mathematical morphology and other statistics [1, 2, 3, 4]. However, applicability of these results to semicontinuous thin film description is limited and other image processing tools have to be used.

The range of growth stages of interest in this contribution is from the later stages of discontinuous thin films, where the island perimeters stop being circular, to the stage where the thin film is soon to become continuous. To our knowledge, there has been no attempt to treat this problem either in physics, or in image processing literature.

In this paper, the problems of semicontinuous thin film segmentation and its natural representation are solved. Signals characterizing the semicontinuous thin film morphology are derived, namely modified tangents of the thin film segment contours, and profiles along the thin film branches. Discrete wavelet transform coefficients of these signals are used to calculate features which describe the semicontinuous thin films in a multiscale and natural manner, and which are easy to interpret.

The paper is organized as follows. Firstly, the concepts of deformable template, skeleton, wavelet transform and feature extraction are introduced and the way they are going to be used is explained. The section with experimental results and discussion follows. Some of the explanations are brief to keep the text to a reasonable length. For more details, references are provided.

2 Image processing tools for semicontinuous thin film image analysis

Thin film segmentation is essential for its coming analysis. A survey of segmentation methods in image processing can be found, for example, in [5]. In cases of highly structured background or noisy images, it is often not clear what the thin film borders are. Another source of difficulty is strongly adherent thin films, where the transition between the thin film and the background is smooth. Then it is difficult to detect the borders precisely without any further knowledge (e.g. about the expected border shape). In this paper, to detect borders at least consistently, they are calculated based on points with maximum slopes, i.e. with extremes in the first derivative.

Segmentation is preceded by an initial normalization to eliminate non-homogeneous image brightness and contrast due to non-ideal imaging. Afterwards, simple thresholding and binary image processing are applied and an initial estimate of the segment contour is obtained. The contour is further refined by means of a deformable template, in this case called a snake. In this contribution, the snakes are used not only for contour refinement, but also for thin film segment skeleton calculation. Therefore, the snakes are more

thoroughly described below.

In case of more complicated thin films, like in the examples presented below, it is natural to represent their spatial distribution by graphs generated by their skeletons. Both the skeleton calculation and its representation are also discussed below.

Both the thin film segment contours and the image intensity profiles along the skeleton branches naturally characterize the thin film. These signals can then be efficiently analyzed by stationary wavelet transform. This is an integral transform increasingly used to describe textures or patterns at different levels of resolution. Based on the transform coefficients, features characterizing the signals and correspondingly also the thin film are calculated. Stationary wavelet transform and the calculated features are explained further in the following sections.

2.1 Contour representation

In this paper, wavelets are used both for processing and approximation of: a) the contour shape, where the contour coordinates are the processed information themselves, and b) the thin film profile which is attributed to a certain curve, corresponding to a skeleton segment.

In digital image processing, the curve/contour coordinates are usually represented by an ordered list of x and y coordinates $(x(s), y(s))$, where s is a sampling along the curve. For later convenience, the sampling should be even.

Another representation used in this paper is equivalent to the angle $\theta(s)$ between the curve and a reference direction. It is constructed so that

$$\theta(s) = \arctan^*(x(s+1) - x(s), y(s+1) - y(s)) \pm 2k\pi \qquad \text{for} \qquad k \in \mathbb{Z},$$

$$|\theta(s+1) - \theta(s)| < \pi,$$

$$\text{and} \qquad \theta(0) \equiv 0.$$

Here, $\arctan^*$ is a four-quadrant inverse tangent and its range is $(-\pi, \pi\rangle$. $\theta(s)$ corresponds to the angle of the curve, adjusted so that there are no large discontinuities arising from the 2π-periodicity of $\arctan^*$.

2.2 Snake

In this paper, the snake is a curve attributed with a linear mass density and developing in time. The snake from [6] is used here. The dynamics of the snake is solved using Hamilton's Integral Principle.

The snake is first initialized. Then it starts moving according to the potential energy, which determines its stretching, bending and moving across the potential field. The acquired kinetic energy is dissipated by means of frictional forces. The ends of the snake can be attached to pre-determined points.

The snake is used here for two tasks. Firstly, it is used to refine the contours. Approximation of the gradient is calculated using the Canny edge detector (see [5]). The scale of the edge detection filter has to be chosen taking into account the contradicting demands of precision and robustness. Then the gradient magnitude is calculated. Taken negatively, it is used as the potential field.

Secondly, the snake is used to calculate the skeleton of a thin film segment. Euclidean distance from the contour, measured inside the segment and taken negatively, is used as the potential field. This makes the snake fall into striations of the field which correspond to the skeleton position. In the case of the skeleton calculation, the positions of the end nodes (the ends of the snakes—see Fig. 1) on the contour have to be pre-determined. This is done by following maxima of the wavelet coefficient magnitudes from coarsest to finest scale, similarly as in, e.g. [7], and using heuristics.

2.3 Skeleton and its representation

It is natural to characterize the spatial distribution of a semicontinuous thin film by means of its skeleton. It is calculated as follows [6]. Between every pair of corners (the pre-determined points) of the segment contours, a single snake is initialized. The snake propagates according to the potential, which is equivalent to the negative Euclidean distance of the inner segment points from the closest contour. The meeting points of different snakes constitute the skeleton, in the sense of this paper.

Compared to some other methods, this approach gives a rotation-invariant skeleton. Moreover, its versatility promises usage in various applications, e.g. in thin film resistance estimation (see [8]).

An example of a skeleton is shown in Fig. 1. It can be represented naturally by a graph, containing a lot of useful structural information. In the figure, it is denoted by marks: what we call an inner node, an end node, an inner branch and an end branch.

The structure of the thin film surface can be well characterized by the image profile p along the skeleton branches. Features calculated on the profile p are explained below. If $(x(s), y(s))$ are coordinates of a skeleton branch and I is the thin film image intensity, then

$$p(s) = I(x(s), y(s)).$$

2.4 Stationary wavelet transform

The features used in this paper are based on stationary wavelet transform (SWT) of the investigated signals. Therefore, it is described in more detail here. Additional details can be found in [9]. SWT is used here because it is shift-invariant. If the original signal is shifted, the transform coefficients are shifted in the same way.

SWT is explained here on a discrete signal $x_0, x_1, \ldots, x_{N-1}$ with length N. Its elements are evenly taken samples of a continuous signal, e.g. a thin film profile. SWT is based on a combination of low-pass and high-pass filtering. Filtering by the low-pass filters H

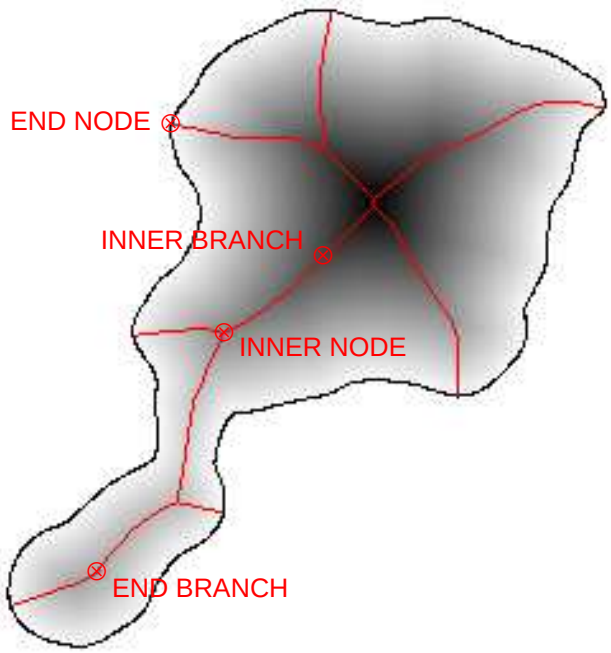

Fig. 1 Euclidean distance transform and skeleton on one particular segment. The distance is measured from the contour inside. It is presented negatively, as it is used for skeleton calculation, i.e. the darker gray level denotes more distant pixels. The image is overlaid by the segment's skeleton together with explanation of terminology.

and the high-pass filters G corresponds to convolving the signal x with reversed filter coefficients h and g, respectively. For example,

$$(Hx)_k = \sum_n h_{n-k} x_n.$$

One-level SWT is then equivalent to the transformation of an initial sequence c^0 (obtained from x—see below; the superscript 0 denotes the initial level) of length N into two signals

$$c^1 = Hc^0 \qquad \text{and} \qquad d^1 = Gc^0,$$

of lengths N.

Since H is a low-pass filter, c^1 is a smoother version of c^0. In the response d^1 to the high-pass filter, information about variation (or details) of the c^0 sequence is stored.

This process can be recursively repeated:

$$c^{i+1} = H^{[i]} c^i \qquad \text{and} \qquad d^{i+1} = G^{[i]} c^i.$$

Filters $H^{[i]}$ and $G^{[i]}$ are derived from the filters H and G, respectively, by inserting $2^i - 1$ zeros between all filter elements. Assume the decomposition is J-level. The original sequence c^0 is thus transformed to c^J, corresponding to the approximation at the coarsest scale J, and to d^1, d^2, …, d^J, corresponding to details at the particular scales.

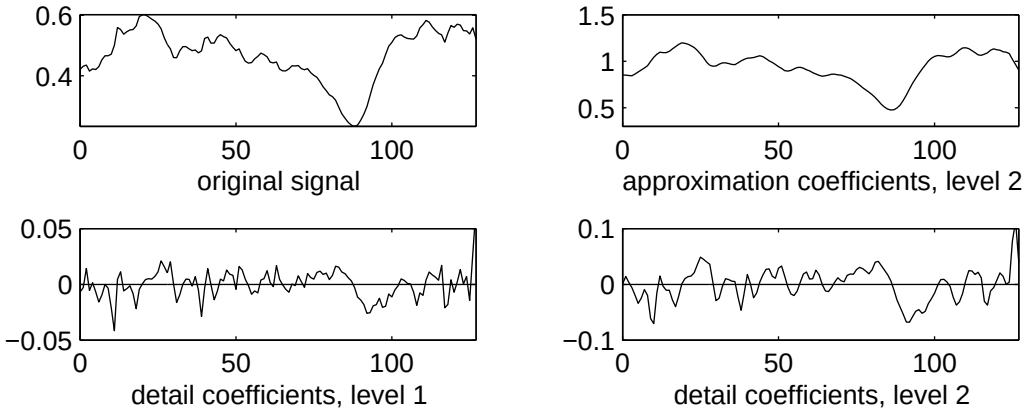

Fig. 2 Example of the SWT decomposition of a one-dimensional thin film profile. The signal is decomposed into 2 levels. All of the detail and approximation coefficients are shown.

The same can be done with the thin film profile. An example of the SWT decomposition of a one-dimensional thin film profile is shown in Fig. 2. However, an initialization usually has to be done, converting the investigated signal x into c^0 (see [10]). Wavelet theory gives a clear interpretation to the coefficients c_k^j and d_k^j. The coefficients c_k^j correspond to projections of the original sequence x on dilations and translations ϕ_{jk} of the so-called scaling function ϕ, where

$$\phi_{jk}(x) = 2^{-j/2}\phi(2^{-j}(x-k)),$$

where j is an index for scaling and k is an index for shifting. Similarly, the coefficients d_k^j correspond to projections of the original sequence x on dilations and translations w_{jk} of the so-called wavelet function w, where

$$w_{jk}(x) = 2^{-j/2}w(2^{-j}(x-k)).$$

Both the scaling function and the wavelet function solve the two-scale dilation equations

$$\phi(x) = 2\sum_k h_k\phi(2x-k)$$

and

$$w(x) = 2\sum_k g_k\phi(2x-k).$$

The dilation equations thus establish correspondence between the filters H and G and the functions ϕ and w.

As can be expected, ϕ is a kind of smoothing function, while w is able to capture signal variation at the corresponding scales. In Fig. 3, the ϕ and w used in this contribution are shown. It can be readily seen from Fig. 2 that the sequences c^2, d^2 and d^1 correspond to the signal magnitudes and variation at particular scales and positions.

Symmetry, number of vanishing moments and regularity are the most relevant wavelet attributes (see [10]). Symmetry (or antisymmetry) simplifies interpretation of the decomposition of the analyzed signal. Regularity ensures reasonable change of the decomposition coefficients when the original signal is shifted. Given the chosen wavelet has q

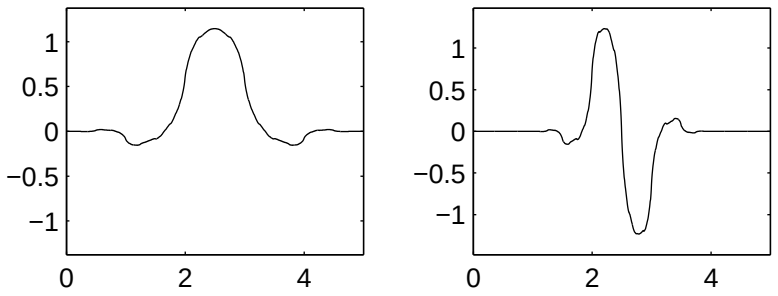

Fig. 3 Scaling function and wavelet used in this paper (bior1.3, [11]).

vanishing moments, the coefficients of the detail responses d are zero if the transformed signal is a linear combination of polynomials up to the $(q-1)$-th order. Therefore, for the detection of an intensity change corresponding to the first derivative, the wavelet should have only one vanishing moment.

3 Feature extraction

The features derived in this paper carry information about thin film morphology. They are calculated on particular branches or contours and also on the whole image.

Invariance of the features under shift, scale change and rotation of the thin film image is desirable. Shift and rotation invariance are ensured by: a) relating some of the features to skeletons which have the same invariance, b) using only the detail coefficients in the case of the signal θ, and c) using features insensitive to the sampling order.

Approximate scale invariance is ensured by an initial re-sampling of the curves. The sampling rate is 2^N samples per length $4L_C$. N is the desired level of decomposition. In case of low resolution, fewer levels are used. L_C is a characteristic size of the thin film, calculated as two times the most probable value of the Euclidean distance along all the thin film branches to the closest contour. L_C is then the most probable width of the thin film branches. It has been experimentally verified that the histogram of Euclidean distances exhibits a relatively sharp single peak. The quantity L_C is thus well defined. Structures with larger L_C are decomposed into more levels. Comparison between feature values is then performed at the corresponding scales.

For ease of interpretation, the wavelet coefficients are normalized, so that a signal scaled in the spatial parameter by the factor 2 would give the same response in the wavelet domain, but at the next scale.

At the end of the J-level wavelet decomposition, every signal (i.e. θ and p) is decomposed into smooth signal c^J and detail signals $d^J, d^{J-1}, \ldots, d^1$. The following features are calculated on the detail signals:

mean absolute value

$$m_A(x) = \frac{1}{K} \sum_{j=1}^{K} |x_j|,$$

energy (the second moment)

$$E(x) = \frac{1}{K}\sum_{j=1}^{K} x_j^2,$$

cross-correlation by means of Pearson's coefficient

$$\rho(x,y) = \frac{\sum x_i y_i}{\sqrt{\sum x_i^2 \sum y_i^2}}, \text{ and}$$

auto-correlation by means of Pearson's coefficient

$$r(x,N) = \rho(x, S^N x).$$

The range of Pearson's coefficient is $\langle -1, 1\rangle$. S^N means a shift by N samples. At the level of decomposition j, N equals 2^j. Correlation is equivalent to covariance here, since the mean of the detail coefficients is usually, in practise, close to zero. It is also usually modeled in this way, and the mean is not subtracted here.

It is difficult to interpret the values m_A and E. Sometimes it is worth evaluating the expression m_A^2/E, further denoted β (see e.g. [12]). Its value is smaller when a few coefficients are significantly higher then the others, i.e. when the structure is sharper. On the other hand, the ratio is higher for smoother structures at a particular scale.

To summarize the set of calculated features, the following features are evaluated at every scale j: $m_A(d^j)$, $E(d^j)$, $\rho(d^j, d^{j-1})$, $r(d^j, 2^j)$ and $\beta(d^j)$. The features are calculated on the signals θ and p. m_A, E and β estimate signal variation, each feature in a different way. The correlation features ρ and r compare variation either at different scales, or for spatially shifted coefficients. In the case of the signal θ, variation corresponds to curvature.

A parameter α can be obtained using Fisher's transformation [13] of Pearson's coefficient and used for comparisons

$$\alpha = \operatorname{arctanh} \rho. \tag{1}$$

It is more natural for comparisons of ρ where $|\rho|$ approaches one. The distribution of the values of α is close to the normal distribution.

For analogous reasons to those for Pearson's coefficient, logarithms of the features m_A and E can be calculated. These also have a distribution close to normal, as has been experimentally verified. The logarithm of β is then simply calculated from the logarithms of m_A and E.

As has been mentioned, the mean and standard deviation of the feature values over the whole thin film image can be calculated. If the features are calculated on the signal θ, the significance of their values varies with the perimeter length of different segments. This is taken into account using weighted mean and weighted standard deviation, where the weight equals the perimeter length.

4 Experimental results

In this section, experimental results are presented and discussed. The experiments were performed on three thin film images, parts of which are shown in the left halves of Figs. 4, 5 and 6.

In the right halves, examples of one particular thin film segment are shown, delineated by the refined contour. The segmentation and contour refinement by means of a snake is described in detail above.

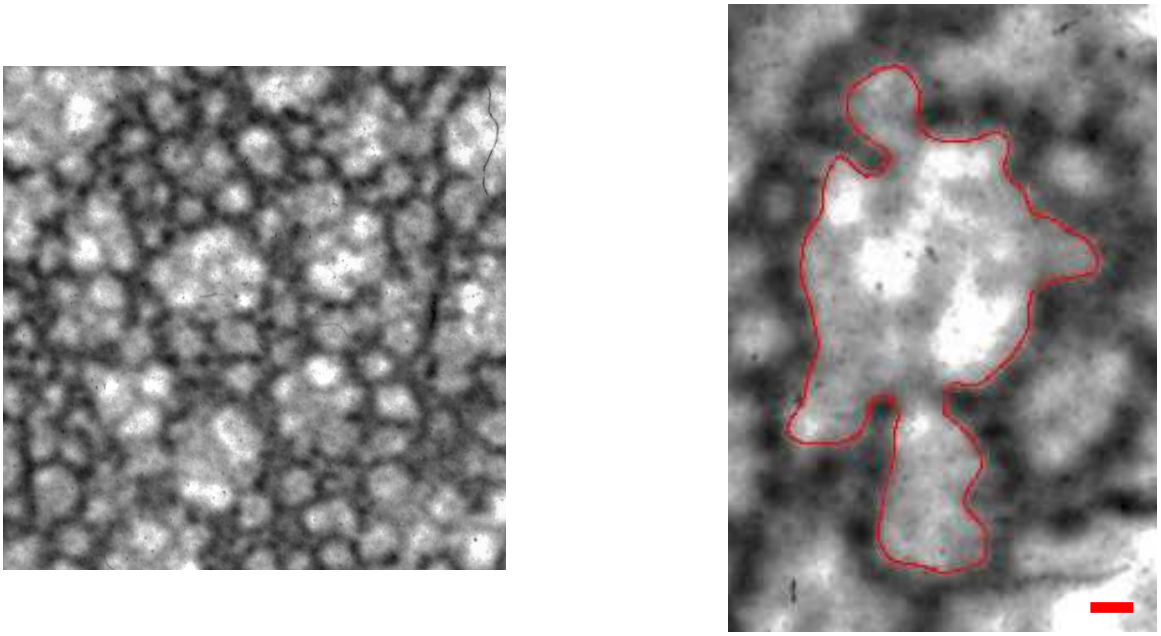

Fig. 4 Example of a thin film number 1. Left: image region of size 600×600 pixels. Right: one particular segment outlined by snake. For comparison, the characteristic length L_C is shown by the thick line.

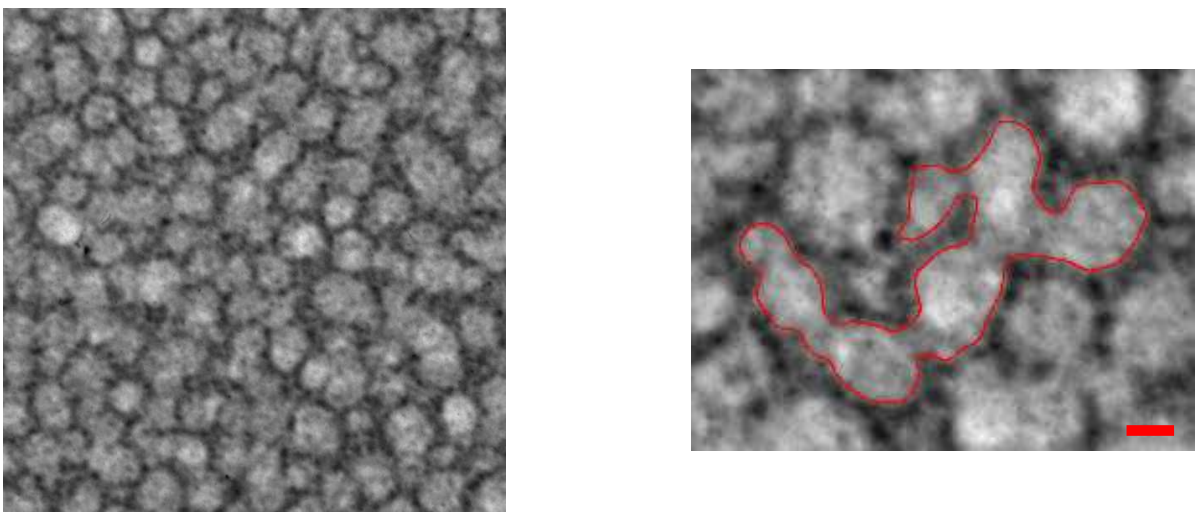

Fig. 5 Example of a thin film number 2. Left: image region of size 600×600 pixels. Right: one particular segment outlined by snake. For comparison, the characteristic length L_C is shown by the thick line.

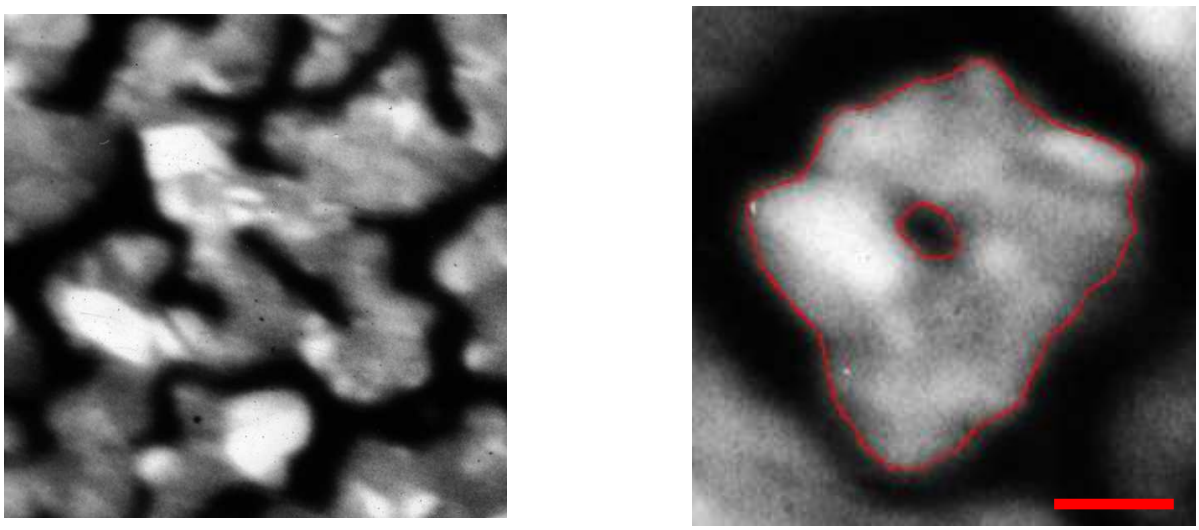

Fig. 6 Example of a thin film number 3. Left: image region of size 600×600 pixels. Right: one particular segment outlined by snake. For comparison, the characteristic length L_C is shown by the thick line.

Subsequently, the skeletons were calculated for all thin film segments with contour length larger then a threshold. This is because for small circular islands it is difficult to determine stable and meaningful corners. The second reason is that the features are either defined for signals corresponding to inner skeleton branches or they require long enough contours. The skeleton of one example segment, corresponding to Fig. 4, is shown in Fig. 7.

In Figs. 8 and 9, typical examples of the signals θ and p are shown. All signals are re-sampled respectively to one characteristic length.

Values of the features m_A, E, ρ, r and β were calculated and are summarized in Tables 1 and 2 for signals θ and p, respectively. The features were calculated for all thin film segments where possible. Afterwards, both the mean and standard deviation of the features were calculated for the whole set of segments contained in one image. If a cell was empty, the statistics could not be calculated. The reasons for this are small resolution of the image, signals which are too short or insufficient number of feature values to calculate the statistics.

First, it has to be pointed out that after all the normalization steps, the three thin films give very similar signals θ and p. Therefore, distinguishing these images is a challenging task. Some of the features give a similar value for these images. Since the characteristics of the separate segments from one image vary as well, the standard deviations are sometimes large. This fact requires proper caution when interpreting or otherwise processing the results. However, even values with large standard deviations can be used in a more complex similarity measure, using the deviations to normalize the differences of the means.

Nevertheless, certain features at certain scales can be found which provide high discrimination power even in this challenging case. Some of these are discussed here, beginning with the signal θ and its feature values contained in Table 1.

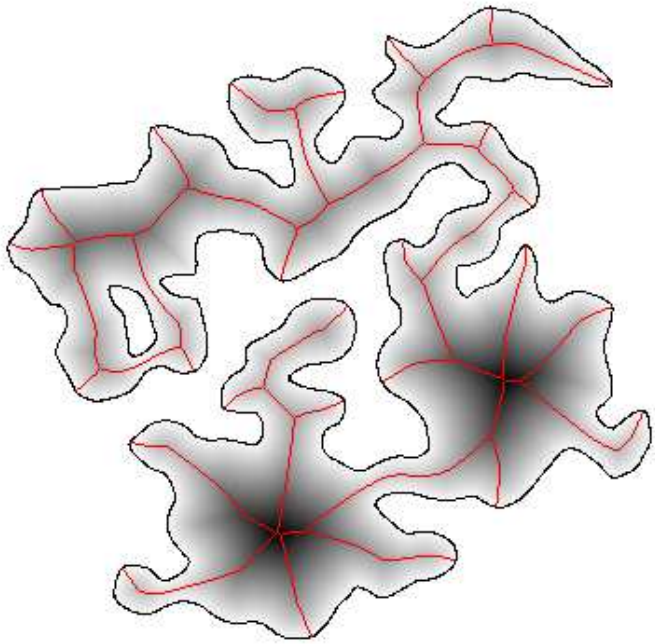

Fig. 7 Skeleton of one particular segment from the thin film number 1. Black line denotes contour, red line denotes skeleton and gray-level values correspond to Euclidean distance from the segment border.

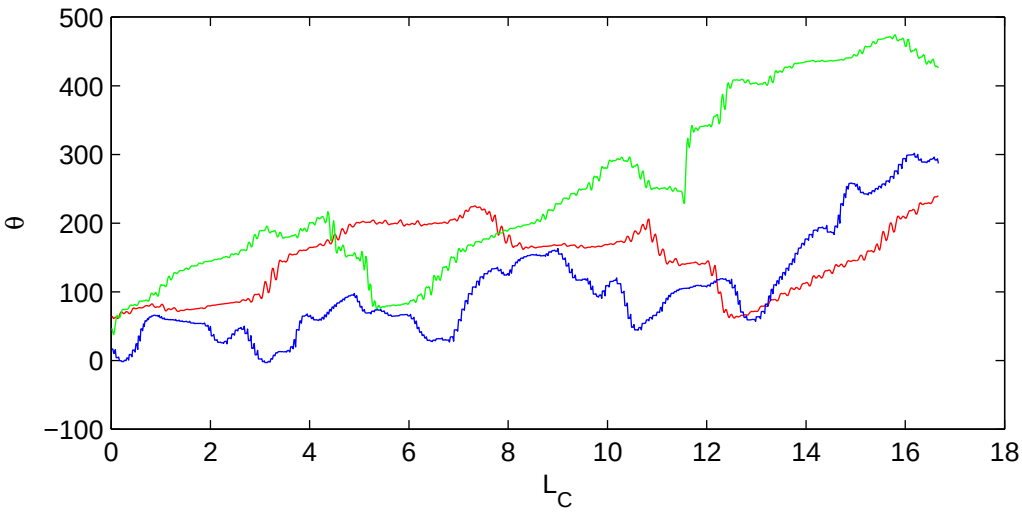

Fig. 8 Segment of the angle signal θ of one particular island from thin film numbers 1 (red), 2 (green) and 3 (blue). It is depicted in units of the characteristic length L_C.

The feature m_A has lower values for image 1 at finer and medium scales. This feature corresponds to the amount of curvature at a particular scale. Therefore, the reason is probably that image 1 contains many larger clusters with respectively lower average curvature.

The values of E are less straightforward to interpret. High value of E can be caused by high curvature on average, or by a few very high coefficients corresponding to locally

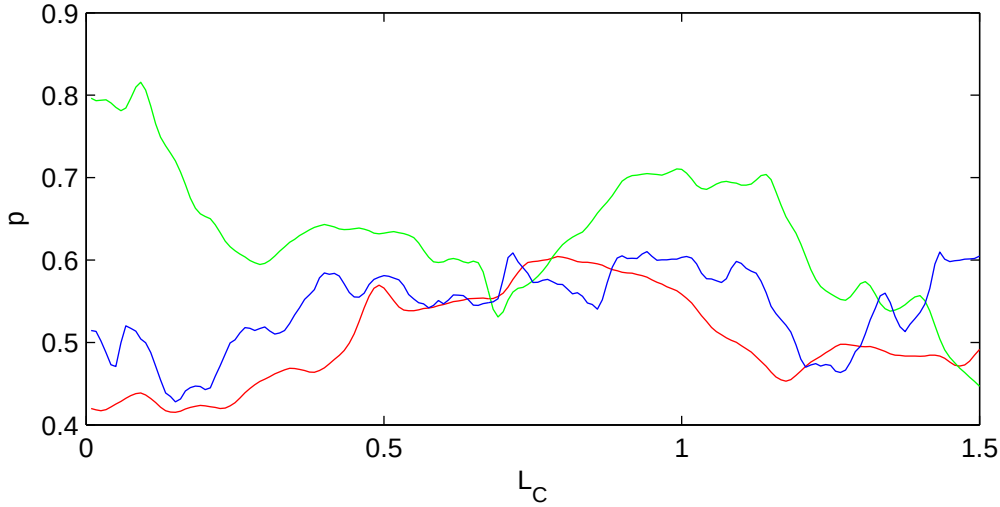

Fig. 9 Segment of the profile signal p of an inner skeleton edge of one particular island from thin films number 1 (red), 2 (green) and 3 (blue). It is depicted in units of the characteristic length L_C.

	1/8	1/4	1/2	1	2
m_A, 1	0.66 ± 0.06	0.95 ± 0.06	1.19 ± 0.05	1.38 ± 0.05	1.50 ± 0.05
m_A, 2	0.80 ± 0.05	1.08 ± 0.05	1.30 ± 0.04	1.45 ± 0.03	1.54 ± 0.03
m_A, 3	0.87 ± 0.05	1.07 ± 0.04	1.26 ± 0.03	1.42 ± 0.03	1.53 ± 0.03
E, 1	1.7 ± 0.1	2.1 ± 0.1	2.58 ± 0.09	2.94 ± 0.09	3.17 ± 0.08
E, 2	1.9 ± 0.1	2.38 ± 0.09	2.78 ± 0.08	3.07 ± 0.05	3.25 ± 0.05
E, 3	2.0 ± 0.1	2.38 ± 0.08	2.72 ± 0.07	3.03 ± 0.05	3.22 ± 0.05
ρ, 1	1.4 ± 0.1	1.8 ± 0.2	1.6 ± 0.1	1.46 ± 0.09	1.2 ± 0.1
ρ, 2	1.6 ± 0.2	1.7 ± 0.1	1.57 ± 0.09	1.24 ± 0.08	1.11 ± 0.07
ρ, 3	1.8 ± 0.2	1.40 ± 0.08	1.3 ± 0.1	1.31 ± 0.09	1.10 ± 0.08
r, 1	0.3 ± 0.2	0.1 ± 0.1	-0.2 ± 0.1	-0.3 ± 0.1	-0.2 ± 0.1
r, 2	0.21 ± 0.09	-0.1 ± 0.1	-0.19 ± 0.09	-0.22 ± 0.09	-0.2 ± 0.1
r, 3	-0.02 ± 0.08	-0.01 ± 0.08	-0.21 ± 0.08	-0.2 ± 0.1	
β, 1	-0.33 ± 0.08	-0.26 ± 0.06	-0.20 ± 0.04	-0.17 ± 0.03	-0.17 ± 0.02
β, 2	-0.30 ± 0.05	-0.22 ± 0.03	-0.18 ± 0.03	-0.16 ± 0.02	-0.16 ± 0.02
β, 3	-0.27 ± 0.06	-0.23 ± 0.05	-0.20 ± 0.02	-0.18 ± 0.02	-0.16 ± 0.01

Table 1 Values of the features m_A, E, β (their logarithms $\log_{10}$) and ρ, r (their α parameters (1)) calculated for the signal θ. The type of feature and image number are denoted in the leftmost column. In the top row, scale is denoted in units of the characteristic length L_C. Differences of points in distance $n\,L_C$ are detected at scale n. Both mean and standard deviation are calculated for the whole set of segments contained in one image.

large curvature. Better insight can be obtained by calculating the feature β. Lower β means sharper characteristics in terms of the curvature (many points with low curvature and some points with large curvature). For example, thin film number 1 seems sharper at finer scales and approximately equally sharp at coarser scales (in the sense of signal θ—see Fig. 8), corresponding to the measured values of β. However, the results must be adopted with caution because of the high values of the standard deviations.

On the other hand, the feature ρ provides fine discrimination in certain cases. The value for image 3 and scale 1/2 is an example worth commenting on. As might be seen from Fig. 8, there is lower correlation for curvature at this scale and the next finer scale, as compared to the other thin films. The feature r is sufficiently discriminative for finer scales.

	1/32	1/16	1/8	1/4	1/2
m_A, 1		-1.9 ± 0.1	-1.6 ± 0.1	-1.4 ± 0.1	-1.2 ± 0.1
m_A, 2		-1.70 ± 0.08	-1.46 ± 0.09	-1.30 ± 0.09	-1.22 ± 0.08
m_A, 3	-1.99 ± 0.05	-1.82 ± 0.07	-1.6 ± 0.1	-1.37 ± 0.08	
E, 1		-3.5 ± 0.2	-3.0 ± 0.2	-2.6 ± 0.2	-2.2 ± 0.2
E, 2		-3.2 ± 0.1	-2.7 ± 0.2	-2.4 ± 0.2	-2.3 ± 0.2
E, 3	-3.8 ± 0.1	-3.4 ± 0.2	-3.0 ± 0.2	-2.5 ± 0.2	
ρ, 1			1.7 ± 0.2	1.5 ± 0.3	1.5 ± 0.2
ρ, 2			1.7 ± 0.2	1.5 ± 0.2	1.2 ± 0.2
ρ, 3		1.3 ± 0.1	1.4 ± 0.3	1.9 ± 0.2	
r, 1		0.2 ± 0.2	0.1 ± 0.2	-0.1 ± 0.2	-0.3 ± 0.2
r, 2		0.1 ± 0.2	-0.2 ± 0.2	-0.3 ± 0.2	-0.2 ± 0.2
r, 3	0.1 ± 0.2	0.3 ± 0.2	0.1 ± 0.3		
β, 1		-0.24 ± 0.09	-0.22 ± 0.08	-0.21 ± 0.08	-0.21 ± 0.05
β, 2		-0.19 ± 0.04	-0.18 ± 0.04	-0.19 ± 0.04	-0.19 ± 0.06
β, 3	-0.21 ± 0.03	-0.22 ± 0.05	-0.21 ± 0.08	-0.24 ± 0.08	

Table 2 Values of the features m_A, E, β (their logarithms $\log_{10}$) and ρ, r (their α parameters (1)) calculated for the signal p. The type of feature and image number are denoted in the leftmost column. In the top row, scale is denoted in units of the characteristic length L_C. Differences of points in distance $n\,L_C$ are detected at scale n. Both mean and standard deviation are calculated for the whole set of segments contained in one image.

Feature values for the signal p are presented in Table 2. Both the features m_A and E suggest that there is more variation at the middle scales for image 2 than for images 1 and 3 (see also Fig. 9). Further, the feature ρ provides good discrimination of the image 3 from the other two images, at the largest measurable scale, again in accordance with Fig. 9. The correlation coefficient r is significantly lower for image 2 and the middle

scales. Fig. 9 suggests that the profile characteristics for this image are rather predictably variable at the characteristic scales under discussion.

It can be concluded that even for these examples which have relatively similar profiles and contour shapes, several sufficiently discriminating features can be found. Some features have large standard deviations to distinguish between the thin films themselves. These can be used in a weighted distance measure, depending on application.

There is no doubt, that a whole class of features with simple intuitive meaning can be derived, based on the graph representation. Further exploitation of the skeleton structure should result in the benefit of finding longer characteristic signals containing several consecutive branches. At the same time, it is possible to use information about widths of thin film branches, measured along the skeleton branches. However, further analysis of all the possibilities would exceed the scope of this paper and is thus left for our future work.

5 Conclusions

A methodology of semicontinuous thin film analysis has been elaborated here. A set of image processing methods has been used for thin film image segmentation, contour refinement, skeleton calculation, and characterization of thin film morphology. A set of features has been calculated, with a clear meaning and good descriptive power, demonstrated on rather challenging thin film images. The results are immediately applicable to real experimental photographs. To the authors' knowledge, similar analysis has not been described yet in the literature.

There are many directions of future interest to us. The graph representation of the skeleton offers the derivation of more extensive and more complex features and information, using results from graph theory. Further, another choice of the end node positions can be used, depending on the application. Another application-dependent issue is the speed of computation, which can be improved at the expense of precision or robustness.

Acknowledgments

This work is part of the research program MSM113200002, Ministry of Education of the Czech Republic. The research has been supported by the grant GAUK-173/2003 of the Grant Agency of Charles University, Prague.

J. Boldyš is currently working in the Laboratory of Media Technology, Department of Automation and Systems Technology, Helsinki University of Technology, Otaniementie 17, 02150 Espoo, Finland.

References

[1] J. Serra: *Image Analysis and Mathematical Morphology*, Academic Press, London, 1982.

[2] B.D. Ripley: *Spatial Statistics*, John Wiley and Sons Inc., New York, 1981.

[3] C.L.Y. Yeong, S. Torquato: "Reconstructing random media", *Physical Review E*, Vol. 57, (1998), pp. 495–506.

[4] R. Hrach, D. Novotný, S. Novák, J. Pavlík: "Multilevel morphological analysis of continuous films and surfaces", *Thin Solid Films*, Vol. 433, (2003), pp. 135–139.

[5] M. Sonka, V. Hlavac and R. Boyle: *Image Processing, Understanding, and Machine Vision*, 2nd ed., PWS, Boston, 1998.

[6] F. Leymarie, M.D. Levine: "Simulating the grassfire transform using an active contour model", *IEEE Transactions on Pattern Analysis and Machine Intelligence*, Vol. 14, (1992), pp. 56–75.

[7] M.I. Khalil, M.M. Bayoumi: "Invariant 2D object recognition using the wavelet modulus maxima", *Pattern Recognition Letters*, Vol. 21, (2000), pp. 863–872.

[8] D. Stauffer and A. Aharony: *Introduction to Percolation Theory*, 2nd ed., Taylor & Francis Ltd., London, 2003.

[9] G. Nason and B. Silverman: "The stationary wavelet transform and some statistical applications", In: *Lecture Notes in Statistics: Wavelets and Statistics*, Springer Verlag, 1995, pp. 281–300.

[10] G. Strang and T. Nguyen: *Wavelets and Filter Banks*, Wellesley-Cambridge Press, Wellesley, 1996.

[11] M. Misiti, Y. Misiti, G. Oppenheim, and J.-M. Poggi: *Wavelet Toolbox User's Guide*, The MathWorks, Inc., 2002.

[12] G. Van de Wouwer, P. Scheunders, D. Van Dyck: "Statistical texture characterization from discrete wavelet representations", *IEEE Transactions on Image Processing*, Vol. 8, (1999), pp. 592–598.

[13] W.H. Press, S.A. Teukolsky, W.T. Vetterling, and B.P. Flannery: *Numerical Recipes in C: The Art of Scientific Computing*, Cambridge University Press, 1992.